REE-bearing minerals in sediment-hosted stratiform pyrite mineralization zones of the Wiśniówka area (Holy Cross Mts., Poland)

Zdzisław M. MIGASZEWSKI[1, *], Agnieszka GAŁUSZKA[1] and Grzegorz ZIELIŃSKI[2]

[1] Jan Kochanowski University, Świętokrzyska 7, 25-406 Kielce, Poland; ORCID: 0000-0001-5549-6224 [Z.M.M.] 0000-0002-2497-2627 [A.G.]

[2] Polish Geological Institute – National Research Institute, Rakowiecka 4, 00-975 Warszawa, Poland, ORCID: 0000-0001-7707-1673

There are two arsenical pyrite (As-FeS$_2$) mineralization zones cropping out in the Podwiśniówka and Wiśniówka Duża quarries where quartzites and quartzitic sandstones have been extracted for over a century. A large amount of pyrite in the Wiśniówka siliciclastics is unusual in the hard rock mining throughout the world. The pyritiferous beds contain a variety of REE-bearing minerals, including a crandallite series of aluminum-phosphate-sulfate (APS) minerals, e.g., predominant goyazite SrHAl$_3$[(PO$_4$)$_2$(OH)$_6$] with subordinate gorceixite BaHAl$_3$[(PO$_4$)$_2$(OH)$_6$] and very occasional crandallite CaHAl$_3$[(PO$_4$)$_2$(OH)$_6$]. By contrast, the other REE-phosphate minerals, e.g., xenotime YPO$_4$, but particularly monazite CePO$_4$, occur in a lesser amount. Goyazite prevails somewhat in the Podwiśniówka beds whereas xenotime in the Wiśniówka Duża beds. Of the other REE-bearing minerals, bastnäsite REECO$_3$(F,OH), florencite (REE)Al$_3$(PO$_4$)$_2$(OH)$_6$ and synchysite CaCe[CO$_3$]$_2$F occur in trace amounts. Interestingly, the quite common phosphate minerals, i.e., wavellite (Al$_3$[(OH,F)$_3$](PO$_4$)$_2$]×5H$_2$O and variscite Al[PO$_4$]×2H$_2$O) are depleted in REEs with only Ce attaining 0.09 wt.% as documented by an electron-probe microanalysis. In contrast to quartzites/quartzitic sandstones, carbonaceous clayey-silty shales and bentonites/tuffites are distinctly enriched in REE-bearing minerals. This diversity is also mirrored in the mean total REE concentrations varying from 204 to 314 mg/kg in clayey-silty shales and bentonites, attaining 457 mg/kg in some Podwiśniówka shale beds. Results of this and the previous petrographic, mineralogical and geochemical studies have indicated that REE-bearing minerals formed generally along with As-rich pyrite, nacrite/dickite and TiO$_2$ polymorphs as a result of multiphase hydrothermal vent activity that took place in the Wiśniówka Late Cambrian sedimentary basin. This evidence is also backed up by the values of LREE$_{NASC}$/HREE$_{NASC}$ (1.44–1.75) and Eu/Eu$_{NASC}$ (1.24–1.30) coefficients in the clayey-silty shales. This positive Eu anomaly (1.20) points to the formation of REE-bearing minerals in a reducing environment.

Key words: siliciclastic rocks, REE-bearing minerals, geochemical analysis, SEM-EDS, EMPA, REE-mineral provenance, Wiśniówka area, Poland.

INTRODUCTION

Due to the growing demand for rare earth elements (REEs) in many areas of industry, especially in electronics and high technologies as well as in agriculture and medicine, the search for and the study of REE mineral deposits have become of crucial importance (e.g., Chakhmouradian and Wall, 2012; Emsbo, et al., 2015; Migaszewski and Gałuszka, 2015). Acid mine drainage (AMD) is a natural process that may enhance the release of REEs from their accessory minerals that occur in bedrock or tailings piles as a result of water-mineral interactions (e.g., Miekeley et al., 1992; Migaszewski and Gałuszka, 2019; Migaszewski et al., 2019; Moreno-González et al., 2020). Hence, to better understand REE behaviour and mobility in AMD environments, we must become more familiar with the occurrence, geochemistry and provenance of primary REE-bearing minerals and their host lithology.

Accessory REE-bearing minerals occur in a wide variety of igneous, metamorphic, hydrothermal and sedimentary settings (e.g., Rasmussen, 1996, 2005; Rasmussen et. al., 1998, 2007; Kositcin et al., 2003; Vallini et al., 2005; Richter et al., 2006; Stanisławska and Michalik, 2008; Harlov et al., 2008; Hetherington et al., 2008; Brański and Mikulski, 2016; Wani, 2017; Mikulski et al., 2021). Of different REE-rich mineral groups, authigenic phosphate (xenotime, monazite) and aluminum-phosphate-sulfate (APS) minerals have been employed in studying sedimentary and diagenetic processes. According to Rasmussen (1996), they represent a significant global sink for
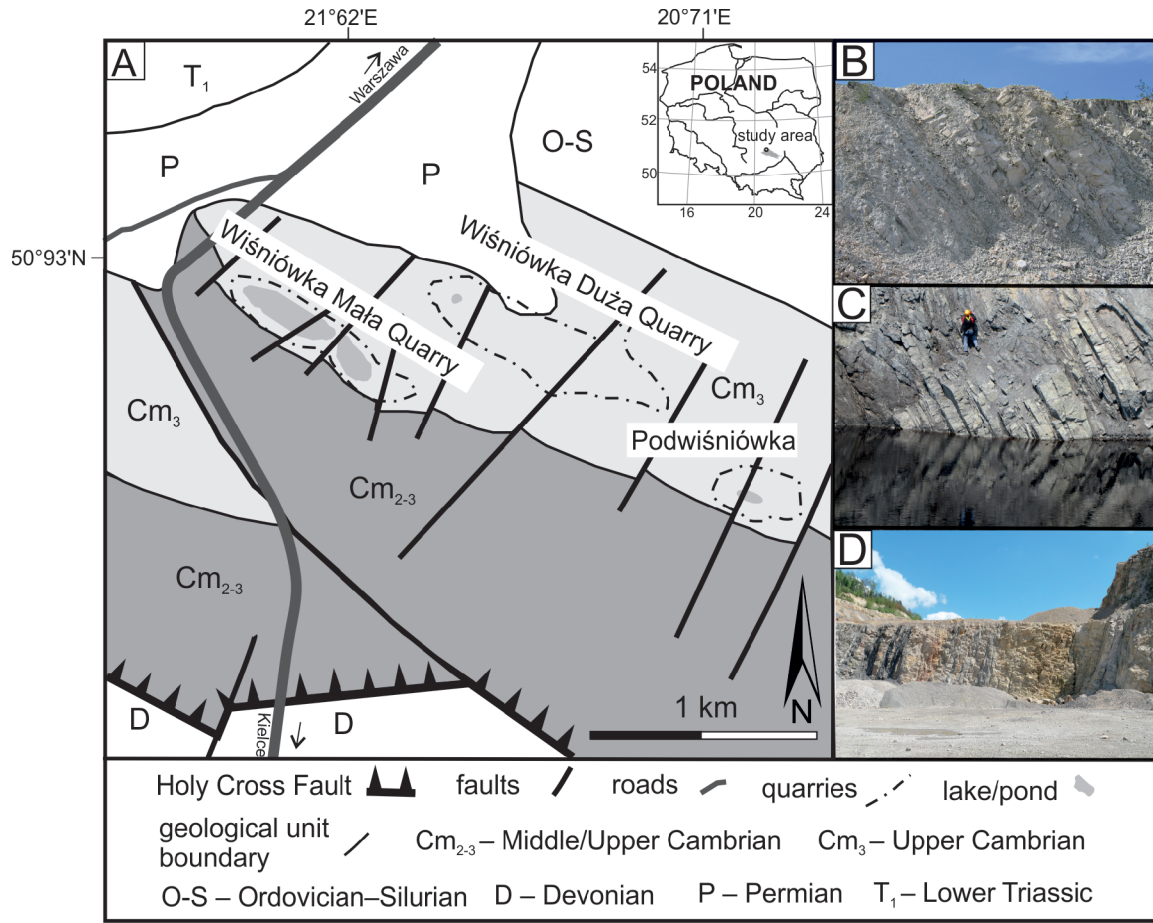
Fig. 1. Geology of the study area with selected outcrops

A – geologic sketch map (modified after Żylińska et al., 2006); B – quartzite-bentonite series in the southwestern part
of the Podwiśniówka Quarry; C – a fragment of quartzite-clayey-silty shale series in the northeastern part of the
Podwiśniówka Quarry; D – eastern part of the Wiśniówka Duża Quarry

oceanic phosphorus, Y and presumably HREEs. Different aspects of geology, mineralogy and geochemistry of APS minerals have been summarized by Dill (2001).

The Wiśniówka area belongs to the unique AMD areas worldwide because of enormous amounts of predominant As-rich pyrite stratiform mineralization zones (unusual in hard rock mining), and additionally the presence of REE-minerals. The previous geochemical, mineralogical and petrographic studies centered primarily around water-mineral interactions in the context of the AMD impact on the neighbouring surface and underground water systems (e.g., Migaszewski et al., 2008, 2013, 2016, 2018a, b, 2019) or plants (Gałuszka et al., 2020). Of the REE-bearing minerals, only gorceixite and xenotime have been described in more detail using optical and scanning electron microscopy (Migaszewski et al., 2007; Migaszewski and Gałuszka, 2010). However, at that time, no electron-probe microanalysis has been performed on xenotime, monazite and APS minerals. Besides, only a small portion of geologic profiles with pyrite mineralization has been exposed in both quarries.

The principal purpose of this study is to summarize the REE rock geochemistry and mineralogy of the Wiśniówka area. To achieve this objective a variety of geochemical and mineralogical methods have been employed including optical and scanning electron microscopy with an energy dispersive spectrometry system (OM, SEM-EDS), electron microprobe analysis (EMPA) and inductively coupled plasma-mass spectrometry (ICP-MS).

MATERIALS AND METHODS

SITE DESCRIPTION

The study area is located in the Wiśniówka massif (western part of the Holy Cross Mts., south-central Poland) within the Upper Cambrian siliciclastic rock formation (Fig. 1A) that consists primarily of alternating beds of quartzites, quartzitic sandstones/siltstones and mostly carbonaceous clayey-silty shales, in places with tuffite and bentonite interbeds (Żylińska et al., 2006; Jaworowski and Sikorska, 2006; Migaszewski and Gałuszka, 2019). This informal regional lithostratigraphic unit, termed the Wiśniówka Sandstone Formation (Orłowski, 1975), is a part of the Łysogóry Block (Łysogóry Unit, Łysogóry Thrust) separated from the Małopolska Block to the south by the Holy Cross Fault (Żylińska et al., 2006; Jaworowski and Sikorska, 2006; Orłowski, 1975; Konon, 2008). The Łysogóry Block (Terrane) borders on the Trans-European Suture Zone (TESZ) that separates the Precambrian East-European Craton from the Paleozoic Platform of Central Europe (Bełka et al., 1997; Konon, 2008; Mazur et al., 2015). In general, most of the geologic profile consists of alternating grey to dark grey, fine-to medium-bedded quartzites/quartzitic sandstones and clayey-silty shales (Fig. 1C, D), and only in the southwestern part of the Podwiśniówka Quarry, they are replaced with light grey, fine-bedded quartzites with numerous tuffite and bentonite interbeds dipping northward (Fig. 1B).

The Wiśniówka area, but especially its eastern part (Podwiśniówka), is characterized by an enormous abundance of stratiform pyrite mineralization giving rise to AMD (e.g., Migaszewski et al., 2008, 2013, 2016, 2018a, b, 2019). Interestingly, the other metal sulfides (galena, sphalerite, tetrahedrite, chalcopyrite, chalcocite, covelline, bornite, cinnabar) and barite are extremely scarce forming inclusions within pyrite and accompanying minerals or host rocks. The principal raw material is quartzite that has been quarried for over a century leaving stone pits, acid water bodies and tailings piles. The oxidation of microcrystalline As-rich pyrite leads to acidification of pit lake and pond waters, the release of metal(loid)s, and subsequently to the formation of various ochreous precipitates in tailings seeps and streams, jeopardizing the neighboring environment (Migaszewski et al., 2018b).

FIELDWORK AND SAMPLING

Geologic fieldwork was conducted for many years as quartzite extraction progressed and included profiling and sampling. For the purpose of this study, 59 rock samples (weighing 0.5–1.0 kg each) were collected from different exposed walls of the Podwiśniówka and Wiśniówka Duża quarries for a more detailed petrographic, geochemical and mineralogical study (Fig. 1). Each sample was placed in a labeled polyethylene bag to prevent accidental mixing. During sampling, transport, storage and treatment, precautions were taken to avoid contamination.

GEOCHEMICAL ANALYSIS AND MICROSCOPE STUDY

Rock samples were used for the geochemical bulk analysis and microscope study. The samples for geochemical analysis were dried at an ambient temperature, and subsequently disaggregated to pass a <0.063 mm screen using a *Pulverisette 2 Fritsch's* blender and an *Analysette 3 Spartan* shaker. The powdered samples were totally digested with a mixture of $HCl + HNO_3 + HF + HClO_4$ (3:2:1:2) and then analyzed for REEs using an ICP-MS; model *ELAN DRC II, Perkin Elmer*. The detection limits for 14 REEs varied from 0.05 (HREEs) to 0.5 mg/kg (LREEs). The certified reference material (CRM) used for measuring lanthanide concentrations was SBC-1, Brush Creek Shale (USGS). Quality control included both accuracy (SRM) and precision (triplicates). The average recovery of REEs from the CRM averaged 80%, the uncertainty of the method was below 10%. The relative standard deviation (RSD) values were <3% for most of the analyzed elements. The geochemical analyses were performed at the accredited Central Chemical Laboratory of the Polish Geological Institute – National Research Institute (PGI–NRI) in Warsaw.

The mineral composition and microtextural features of rock samples were examined using a stereoscopic microscope *Leica M205A* and a petrographic microscope *Nikon LV 100 Pol*. The microscope studies were performed on raw rock chips and polished thin sections, respectively. These optical microscope analyses were carried out at the Environmental Analytical Laboratory, Jan Kochanowski University in Kielce.

The rock samples were also examined with a scanning electron microscope combined with an energy dispersive spectrometer (SEM-EDS); model *LEO 1430, Carl Zeiss Jena*. The following measuring parameters were applied: signal A – backscattered electron (BSE) and secondary electron (SE1), magn. 1260–15,850 , accelerating voltage (EHT) 20.00 kV, working distance (WD) 10–21 mm. Concentrations of REEs, Al, As, Ba, Cl, Cr, F, Fe, K, Mg, Mn, Na, P, S, Si and Sr in selected rock samples were in turn determined using an electron microprobe analyzer (EMPA), model *Cameca SX-100* equipped with four wavelength dispersive detectors. The measuring parameters included: accelerating voltage 15 kV, probe current 20 nA, beam diameter 1 to 5 µm and BSE signal. These studies were done on carbon-coated polished thin sections. The microanalysis was performed at the Microanalysis Laboratory of the Polish Geological Institute – National Research Institute in Warsaw.

For the purpose of this study, the authors divided REEs (lanthanides) into two subgroups: light REEs (LREEs; La through Eu) and heavy REEs (HREEs; Gd through Lu). The third subgroup, middle REEs (MREEs; Sm through Dy), overlaps both LREEs and HREEs. The REE anomalies were identified after normalization of REE concentrations to North American Shale Composite/NASC (Haskin et al., 1968; Gromet et al., 1984). The Ce/Ce$_{NASC}$* coefficient in the Wiśniówka rock samples was calculated from the equation (1) given by Bau and Dulski (1996) and reported in Table 1:

$$Ce/Ce_{NASC}{}^{*} = Ce_{NASC}/(0.5La_{NASC} + 0.5Pr_{NASC}) \qquad [1]$$

where: $Ce_{NASC}{}^{*}$ – a background concentration whereas La_{NASC} and Pr_{NASC} are the NASC-normalized La and Pr concentrations, respectively.

The similar equation was employed for the Eu/Eu$_{NASC}$* coefficient. To calculate the Eu anomaly, two neighboring elements, i.e., Sm and Gd, were included in the equation (2) as reported by German et al. (1991):

$$Eu/Eu_{NASC}{}^{*} = Eu_{NASC}/(0.5\,Sm_{NASC} + 0.5Gd_{NASC}) \qquad [2]$$

Values 0.8 are indicative of negative anomalies whereas those 1.2 point to positive anomalies (Grawunder et al., 2014; Migaszewski et al., 2016). This ±0.2 range is linked to the measurement error. This implies that values in the range of 0.81 to 1.19 are not regarded as anomalies.

RESULTS AND INTERPRETATION

BULK CONCENTRATIONS OF REES AND Y IN MAIN ROCK TYPES

Observed mean and range concentrations of REEs and Y as well as NASC-normalized REE concentration coefficients in main lithotypes of the Podwiśniówka and Wiśniówka Duża quarries are summarized in Table 1. Both REEs and Y predominate in clayey-silty and bentonite facies of the Wiśniówka Formation as opposed to quartzites/quartzitic sandstones which are distinctly depleted in these elements. The highest total REE concentrations occur in carbonaceous clayey-silty shales of Podwiśniówka varying from 131 to 457 mg/kg with a mean of 314 mg/kg. Similarly, these rocks also contain Y ranging from 8.3 to 31.8 mg/kg with a mean of 18.5 mg/kg. These REE concentrations are higher than those in the Continental Crust (144.3 mg/kg; Wedepohl, 1995) or the Upper Continental Crust (146.37 mg/kg; Taylor and McLennan, 1985). By comparison, the carbonaceous shales of the Cu-rich sections of the Kupferschiefer copper deposit in Poland contain REEs and Y in the range of 117 to 158 mg/kg and 12 to 23 mg/kg Y, respectively (Sawłowicz, 2013). Similarly, in Maastrichtian carbonaceous claystones of the Haymana formation (Turkey) lesser amounts of REEs (range of 77.81 to 162.05 mg/kg, mean of

Observed mean (±SD) and range REE and Y concentrations and NASC-normalized REE concentration coefficients in main lithotypes of the Podwiśniówka and Wiśniówka Duża quarries

REE concentrations /REE ratios	Podwiśniówka			Wiśniówka Duża	
	Shales (N=22)	Bentonites (N=6)	Quartzites (N=17)	Shales (N=9)	Quartzites (N=5)
REE (La–Lu) (mg/kg)	314±40.7 (131–457)	235±29.2 (163–333)	105±13.6 (39–265)	204±25.9 (155–271)	97±12.3 (75–126)
LREE (La–Eu) (mg/kg)	295±52.6 (123–432)	216±37.8 (141–310)	98.9±17.6 (66–252)	190±33.6 (151–254)	90.5±16.0 (69–117)
HREE (Gd–Lu) (mg/kg)	19.4±2.61 (7.92–33.6)	18.7±2.40 (11.9–23.3)	5.91±0.799 (2.91–13.4)	14.1±1.65 (12.5–17.5)	6.78±0.807 (5.61–9.44)
Y (mg/kg)	18.5±5.25 (8.3–31.8)	18.2±5.22 (11.8–25.0)	5.93±2.01 (3.7–11.1)	16.3±2.61 (11.5–21.1)	8.08±2.04 (6.7–11.6)
$LREE_{NASC}/HREE_{NASC}$	1.75	1.36	1.89	1.44	1.44
Ce/Ce_{NASC}^{*}	1.09	1.06	1.09	1.02	1.04
Eu/Eu_{NASC}^{*}	1.30	1.20	1.12	1.24	1.04
La_{NASC}/Yb_{NASC}	2.47	2.01	2.76	1.98	1.95
La_{NASC}/Sm_{NASC}	1.02	0.95	0.94	1.17	1.03
La_{NASC}/Gd_{NASC}	1.41	1.13	1.47	1.55	1.42
Sm_{NASC}/Yb_{NASC}	2.42	2.13	2.93	1.69	1.90

110.82 mg/kg) have been determined (Koç et al., 2016). In another study of the epicontinental Polish Basin sediments, concentrations of total REEs in the uppermost Triassic mudstones and claystones (borehole Niekłań IG 1) have been more diversified varying from 34.1 to 2450.1 mg/kg (mean of 560.6 mg/kg) whereas in the Lower Jurassic mudstones and claystones from 136.0 to 509.6 mg/kg (max. value in borehole Kaszewy 1) with a mean of 223.4 mg/kg (Brański and Mikulski, 2016).

The lowest REE levels varying from 75 to 126 mg/kg (mean of 97 mg/kg) have been recorded in Wiśniówka Duża quartzites/quartzitic sandstones. These values are generally higher than those in Proterozoic sandstones (13 to 76 mg/kg) and quartzites (24.77 to 323.6 mg/kg) of southeastern India (Wani, 2017). This commonly encountered dissimilarity in REE contents between main lithotypes is induced not only by a decreased amount of REE-bearing minerals, but presumably also by a substantial drop of clay minerals and organic matter. The abundances of REEs and additionally Y range several order of magnitude within individual beds, especially in the Podwiśniówka host rocks. The most distinct variations in REE concentrations (39–265 mg/kg) have been noted between individual Podwiśniówka quartzite/quartzitic sandstone interbeds. Yttrium also shows diverse concentrations between individual rock beds of both quarries; however, the most considerable variation (range of 8.3 to 31.8 mg/kg) has been found in Podwiśniówka clayey-silty shales.

It is interesting to compare total concentrations of two REE subgroups in the Wiśniówka Formation. Both in the Podwiśniówka and Wiśniówka Duża quarries, measured LREEs pronouncedly prevail over HREEs. This relationship is more highlighted by the $LREE_{NASC}/HREE_{NASC}$ coefficient varying from 1.36 (Podwiśniówka bentonites) to 1.89 (Podwiśniówka quartzites/quartzitic sandstones). Interestingly, both clayey-silty shales and quartzites/quartzitic sandstones of Wiśniówka Duża show the lower $LREE_{NASC}/HREE_{NASC}$ coefficient averaging 1.44 than those in Podwiśniówka (1.75–1.89). This is also evidenced by the La_{NASC}/Yb_{NASC} coefficient of these two lithotypes of Wiśniówka Duża that ranges from 1.95 to 1.98.

Podwiśniówka bentonites exhibit nearly the same $LREE_{NASC}/HREE_{NASC}$ (1.36) and La_{NASC}/Yb_{NASC} (2.01) coefficients. Both lower values suggest that clayey-silty shales and quartzites/quartzitic sandstones od Wiśniówka Duża as well as bentonites of Podwiśniówka are somewhat enriched in HREEs compared to Podwiśniówka clayey-silty shales. Similar results have been derived from the previous study on a lesser amount of samples (Migaszewski and Gałuszka, 2019). Of the two redox-sensitive elements, i.e., Ce and Eu, only Eu shows a significant positive anomaly (1.2) in clayey-silty shales and bentonites. The other coefficients commonly used to determine a contribution of MREEs (Sm through Dy), e.g., La_{NASC}/Gd_{NASC} and Sm_{NASC}/Yb_{NASC} seem to be of doubtful significance due to the sharp decrease of REE concentrations at the boundary between Eu and Gd (Fig. 2).
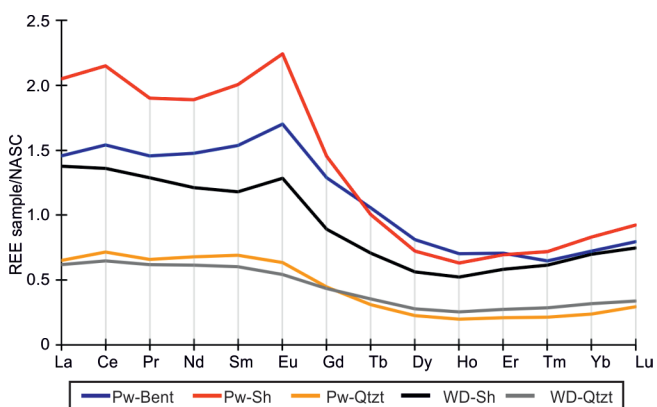
Fig. 2. NASC-normalized REE concentration patterns on a logarithm scale of Podwiśniówka and Wiśniówka Duża main lithotypes

Pw-Sh – Podwiśniówka clayey-silty shales, Pw-Bent – Podwiśniówka bentonites, WD-Sh – Wiśniówka Duża clayey-silty shales, Pw-Qtzt – Podwiśniówka quartzites, WD-Qtzt– Wiśniówka Duża quartzites

MINERALOGICAL AND GEOCHEMICAL CHARACTERISTICS OF REE-BEARING MINERALS

Microtextures of REE-bearing minerals are depicted in Figures 3 and 4, whereas their chemical composition is given in Tables 2, 3 and 4. Goyazite $SrHAl_3[(PO_4)_2(OH)_6]$ is a predominant REE-bearing mineral in the Wiśniówka area. The other APS minerals, i.e., gorceixite $BaHAl_3[(PO_4)_2(OH)_6]$, but particularly crandallite $CaHAl_3[(PO_4)_2(OH)_6]$, are very scarce. However, some beds comprise more gorceixite than the remaining APS minerals (Migaszewski et al., 2007). Goyazite assemblages usually do not exceed 100 μm in diameter and commonly reveal a heterogeneous microtexture composed of light grey rhombohedral or cubic cores floating in a grey matrix (Fig. 3C). This mineral infills interstitial micropores or microcracks between quartz grains (Fig. 3A, B). In places, goyazite shows a more complex microtexture that consists of grey aggregates and embedded crystals with alternating wide light grey and thin grey microbands (Fig. 3C). The light grey core or band domains are distinctly enriched in LREEs attaining 21.00 wt.% whereas the grey matrix is depleted in LREEs generally averaging <1 to 3 wt.%. The LREE subgroup is represented by La (up to 10.39 wt.%), Ce (up to 8.90 wt.%), Nd (1.54 wt.%) and subordinate Sm (0.17 wt.%).

According to Rasmussen et al. (1998), APS minerals and apatite are enriched in LREEs as opposed to xenotime that concentrates HREEs (discussed below). Some goyazite aggregates partially fill the interior of microfossils (Fig. 3E). It is interesting to note that APS minerals also make up transitional forms from goyazite to gorceixite or crandallite within individual grains, which is evidenced by results of microanalysis performed on sample WD2 (Fig. 3G and Table 4). The contents of Sr, Ba and Ca are in the range of 4.14–4.47 wt.%, 1.46–4.37 wt.% and 1.62–2.22 wt.%, respectively. This Sr-Ba-Ca-APS mineral grain also shows enrichment in LREEs (Ce > Nd > La > Sm) varying from 8.95 to 12.31 wt.% (Table 4). Goyazite and subordinate gorceixite and crandallite assemblages occur occasionally in the form of paragenetic occurrences with pyrite (Fig. 3F–H) or goethite, TiO_2 polymorphs and nacrite/dickite (Fig. 3D).

It is also interesting to compare concentrations of REEs and accompanying elements in goyazite and gorceixite aggregations (Table 2). For example, goyazite shows variable contents of major elements: 10.05 to 18.19 wt.% (Al), <0.1 to 4.37 wt.% (Ba), 0.46 to 2.22 wt.% (Ca), 6.41 to 12.61 wt.% (P), 0.22 to 4.04 wt.% (S) and 1.51 to 7.65 wt.% (Sr) (Table 2). The REE contents also exhibit the same substantial variations as exemplified by Ce (4.25 to 10.43 wt.%), La (1.31 to 8.90 wt.%), Nd (1.15 to 5.41 wt.%) and subordinate Sm (<0.1 to 0.77 wt.%; Table 3). The variability of minor and trace elements is also found within some gorceixite grains, but like in goyazite, there is no interrelationship between element contents and microtextural patterns. Among APS minerals, gorceixite is distinguished by the highest content of Ba varying from 9.89 to 26.80 wt.% (mean of 20.89 wt.%), Cl from <0.1 to 4.44 wt.% (mean of 0.45 wt.%) and F in the range of 0.21 to 1.64 wt.% (mean of 0.97 wt.%; Table 2). However, as opposed to goyazite, gorceixite contains a lesser amount of REEs reaching 4.85 wt.% (Table 3). It should be stressed that APS minerals do not contain arsenic although very high concentrations of this element have been recorded in pyrite (up to 8.2 wt.%; Migaszewski et al., 2016) and goethite/hematite (up to 5.29 wt.%; Migaszewski and Gałuszka, 2019).

The second most widespread REE-rich mineral in the Wiśniówka area is xenotime forming mostly syntaxial tooth-like overgrowths up to 70 μm in diameter on detrital zircon grains (Fig. 4A–D). In places, the xenotime rim is nearly complete (Fig. 4A, B). Most of the outer surfaces of xenotime overgrowths exhibit no rounded morphologies, thus precluding the transport of combined zircon/xenotime aggregates from the proximal parts of the shelf. Xenotime occurs also as discrete grains locally composed of 2–3 generations (Fig. 4E, F). In some places, xenotime fills microcracks or micropores within zircon grains. The boundaries between xenotime generations of composite assemblages show locally etching that may result from early-diagenetic dissolution by hydrothermal fluids (inner tooth-like rims; Fig. 4E). In contrast, the outer rims reveal typically a strong dissolving pattern derived from reactive pyrite oxidation products (outer rims). The light grey domains contain more HREEs and U compared to their grey and dark grey equivalents (Migaszewski and Gałuszka, 2019). Xenotime assemblages occasionally show a delicate irregular zonal and/or patchy microtextures similar to those observed in goyazite. In xenotime, in contrast to the APS minerals, phosphorus reveals a more uniform spatial distribution, varying from 13.73 to 15.46 wt.% with a mean of 15.00 wt.% (Table 2). Of the REE-rich minerals, xenotime comprises the largest amount of HREEs with an admixture of some LREEs (Nd, Sm, Eu) (Table 3). The total mean content of HREEs amounts to 17.09 wt.% whereas LREEs to 0.92 wt.%. This mineral shows the following sequence of mean HREE concentrations (wt.% in parentheses): Dy (5.66) > Er (3.16) > Gd (2.94) > Yb (2.81) > Ho (1.00) > Tb (0.65) > Lu (0.59) > Tm (0.28). The same HREE trend is seen in single xenotime grains (Table 4). The most enriched in total REEs (22.5 wt.%) and HREEs (21.25 wt.%) is a xenotime grain that has been found is sample WD2 from the Wiśniówka Duża Quarry.

Another REE-phosphate mineral is monazite $CePO_4$ that occurs in a minor amount. It forms individual grains devoid of banded or patchy microtextures (Fig. 4G). Like in xenotime, the concentration of phosphorus in this mineral shows relatively small variations from 11.84 to 13.44 wt.% with a mean of 13.09 wt.% (Table 2). REEs are represented primarily by LREEs with a following sequence of mean values (wt.% in parentheses): Ce (25.86) > La (13.35) > Nd (9.69) > Pr (2.54) > Sm (1.34) > Eu (0.10). HREEs encompass only Gd (1.10 wt.%) and Dy (0.42 wt.%). The highest total contents of total REEs (58.14 wt.%) including LREEs (57.23 wt.%) have been noted in sample Pw39 from the Podwiśniówka Quarry. Monazite also shows enrichment in yttrium in the range of 0.16 to 2.49 wt.% (mean of 1.38 wt.%). As opposed to most APS and xenotime occurrences, monazite grains show distinct cracking and etching of rims induced by reactive pyrite oxidation products (Fig. 4G). Monazite forms predominantly authigenic assemblages as opposed to detrital grains which are extremely scarce.

Of the other REE-bearing minerals, bastnäsite $REECO_3(F,OH)$, florencite $(REE)Al_3(PO_4)_2(OH)_6$ and synchysite $CaCe[CO_3]_2F$ are extremely scarce or negligible. Interestingly, the quite common phosphate minerals, i.e., brownish wavellite $(Al_3[(OH,F)_3](PO_4)_2 \times 5H_2O)$ (Fig. 4H) and pale green variscite $(Al[PO_4] \times 2H_2O)$, are depleted in REEs in relation to APS minerals, xenotime and monazite as evidenced by an electron microprobe examination. REEs are represented by cerium not exceeding 0.10 wt.% in these two minerals (Table 3). The major elements, e.g., Al and P, show slightly variable concentrations with mean values of 18.92 wt.% (Al) and 15.68 wt.% (P) in wavellite and 17.24 wt.% (Al) and 19.17 wt.% (P) in variscite (Table 2)
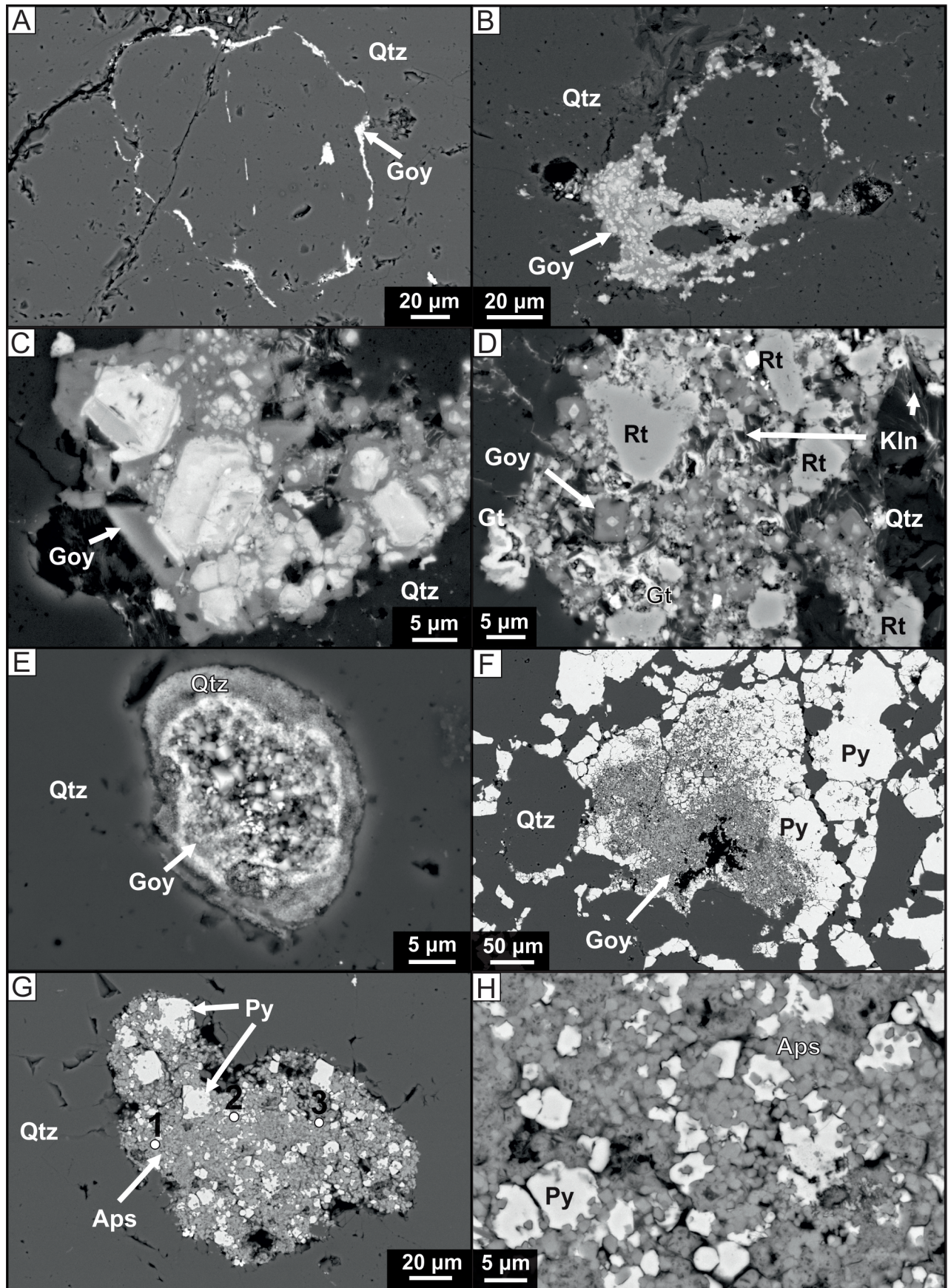
Fig. 3. Back-scattered SEM photomicrographs of APS minerals

A – goyazite assemblages infilling microcracks along quartz grain boundaries roughly patterning a map of Poland (sample Pw10); **B** – goyazite aggregates composed of LREE-rich cores (light grey) and LREE-depleted matrix infilling microvoids between quartz grains (sample Pw3, 11.5–11.6 m); **C** – a goyazite aggregate showing mostly a zonal-patchy microtexture with LREE-rich (light grey) and LREE-poor domains (grey; sample Pw3, 11.5–11.6 m); **D** – a mixed aggregation of goyazite, kaolinite, goethite and rutile (sample Pw3/1); **E** – a microfossil (acritarch?) infilled with a goyazite aggregate rimmed with a silica sheath (sample Pw15); **F** – goyazite being partly replaced wit a pyrite assemblage (sample Pw20); **G**, **H** – a transitional APS assemblage (goyazite-gorceixite-crandallite; see Table 4) with scattered interlocked pyrite inclusions (sample WD2); Anh – anhydrite, Aps – aluminum-phosphate-sulfate minerals, Goy – goyazite, Gt – goethite, Kln – kaolinite (nacrite/dickite), Mnz – monazite, Py – pyrite, Qtz – quartz, Rt – rutile; Wvl – wavellite, Xnt - xenotime, Zrn – zircon

Mean and range contents of major and minor elements in REE-bearing minerals of the Wiśniówka area (derived from EMPA)

Element [wt.%]	Goyazite (N = 87)	Gorceixite (N = 20)	Xenotime (N = 62)	Monazite (N = 18)	Wavellite (N = 35)	Variscite (N = 22)
Al	15.66 0.98 10.05–18.19	14.82 1.00 11.40–15.70	bdl	bdl	18.92 0.77 17.61–20.65	17.24 0.44 16.43–18.07
Ba	0.54 0.64 <0.1–4.37	20.89 6.92 9.89–26.80	bdl	bdl	0.02 0.03 <0.1–0.11	bdl
Ca	0.98 0.36 0.46–2.22	0.27 0.34 <0.1–1.42	0.20 0.15 <0.1–0.71	0.51 0.20 0.05–0.74	<0.1–0.02	0.02 0.01 0.1–0.04
Cl	bdl	0.45 1.08 <0.1–4.44	bdl	bdl	bdl	bdl
F	0.29 0.09 0.12–0.60	0.97 0.32 0.21–1.64	bdl	bdl	2.41 0.96 0.29–3.71	0.29 0.04 0.22–0.41
Fe	0.48 0.50 <0.1–2.04	3.96 7.06 <0.1–20.52	0.13 0.26 <0.1–1.44	<0.1–0.06	bdl	0.09 0.02 bdl
K	<0.1–0.13	<0.1–0.15	bdl	bdl	bdl	bdl
Mg	<0.1–0.16	bdl	bdl	bdl	bdl	bdl
Mn	bdl	0.24 0.55 <0.1–2.23	bdl.	bdl	bdl	bdl
Na	<0.1–0.11	0.10 0.05 0.1–0.22	bdl	bdl	bdl	bdl
P	11.17 0.77 6.41–12.61	8.53 4.39 0.98–11.62	15.00 0.33 13.73–15.46	13.09 0.38 11.84–13.44	15.68 0.41 14.74–16.41	19.17 1.09 17.29–20.86
S	0.89 0.59 0.22–4.04	0.80 1.80 <0.1–8.40	<0.1–0.15	<0.1–0.17	bdl	bdl
Si	0.28 0.30 <0.1–2.38	0.54 0.32 0.16–1.44	0.36 0.23 <0.1–1.17	0.19 0.19 0.07–0.88	bdl	bdl
Sr	4.01 1.11 1.51–7.65	1.07 1.95 0.10–6.92	bdl	bdl	bdl	bdl

bdl – below detection limit; (~0.1 wt.%); arsenic and chromium always occurs below detection limit; when the number of points containing a specific element below detection limit amounted to more than 20% of the total number of points, then only observed concentration ranges are given

Another interesting issue is a concentration of REEs in accompanying authigenic assemblages of pyrite, goethite/hematite or TiO_2 polymorphs. Electron-probe microanalysis has shown that these elements occur only in trace amounts and are represented only by Ce reaching 0.27 wt.% in TiO_2 polymorphs.

DISCUSSION

RARE EARTH ELEMENTS FINGERPRINTING SEDIMENTARY CONDITIONS

The NASC-normalized REE concentration patterns of principal rocks types in both Podwiśniówka and Wiśniówka Duża quarries are depicted in Figure 2. Five linear graphs confirm enrichment of lithotypes in LREEs, which is also evidenced by the $LREE_{NASC}/HREE_{NASC}$ and La_{NASC}/Yb_{NASC} coefficients (discussed in subsection Bulk concentrations of REEs and Y in main rock types). Both Ce and Eu anomalies may indicate the redox conditions during the formation of REE-rich minerals. In seawater at moderately elevated pH and/or Eh, Ce^{3+} oxidizes to lower soluble Ce^{4+} (Dia et al., 2000; Leybourne et al., 2000). Consequently, this cation undergoes precipitation giving a positive anomaly in sediments/rocks (Brookins, 1989; Atlas, 2005; Migaszewski and Gałuszka, 2015). Europium exhibits the op-

posite behaviour, this means that Eu^{3+} is reduced to insoluble Eu^{2+} at low Eh (below 350 mV) and/or pH in very reducing aqueous environments. Taking together, both negative Ce and positive Eu anomalies in waters indicate the oxidizing conditions and *vice versa* the reducing conditions. However, in sediments/rocks, Ce and Eu show inversely proportional patterns under the same conditions. Nonetheless, this relationship is distorted in the submarine hydrothermal systems (discussed later).

In the Wiśniówka area clayey-silty shales exhibit a distinct positive Eu anomaly varying from 1.24 (Wiśniówka Duża) to 1.30 (Podwiśniówka). This coefficient points to a reducing environment during the formation of REE-bearing minerals, which is also evidenced by the presence of dominant dark grey to black carbonaceous clayey-silty shales hosting scattered microcrystalline pyrite, as well as the V/(Ni+V) ratio. Results of the previous study (Migaszewski and Gałuszka, 2019) have shown that Podwiśniówka dark grey to black pyritiferous, carbonaceous clayey-silty shales are distinctly enriched in total organic carbon/TOC (range of 0.13 to 1.54%) compared to their Wiśniówka Duża equivalents (range of <0.10 to 0.35%). It is noteworthy that pyrite-rich carbonaceous shales of the Haymana formation in Turkey are also abundant in TOC in the range of 0.39 to 1.69% (Acar et al., 2007) and they also show a strongly positive Eu anomaly (Fig. 4 in Koç et al., 2016). In con-

T a b l e   3

Mean and range contents of REEs and Y in APS and phosphate minerals of the Wiśniówka area (derived from EMPA)

Element [wt.%]	Goyazite (N = 87)	Gorceixite (N = 20)	Xenotime (N = 70)	Monazite (N = 22)	Wavellite (N = 35)	Variscite (N = 22)
Y	bdl	0.12 0.06 <0.1–0.22	32.83 1.47 29.02–38.19	1.38 0.68 0.16–2.49	bdl	bdl
La	3.38 1.62 1.31–8.90	0.10 0.19 <0.1–0.61	bdl	13.35 1.83 10.07–17.37	bdl	bdl
Ce	7.84 1.46 4.25–10.43	1.24 0.59 0.16–2.44	bdl	25.86 1.29 23.88–28.03	bdl <0.1–0.1	bdl <0.1–0.1
Pr	bdl	bdl	bdl	2.54 0.15 2.26–2.94	bdl	bdl
Nd	2.96 0.85 1.15–5.41	0.20 0.43 <0.1–1.51	0.26 0.12 <0.1–0.65	9.69 0.61 9.00–11.59	bdl	bdl
Sm	<0.1–0.77	<0.1–0.44	0.66 0.28 0.06–1.56	1.34 0.32 0.73–1.98	bdl	bdl
Eu	bdl	bdl	0.28 0.19 <0.1–0.71	0.10 0.09 <0.1–0.36	bdl	bdl
Gd	bdl	bdl	2.94 1.51 0.53–7.25	1.10 0.29 0.48–1.57	bdl	bdl
Tb	bdl	bdl	0.65 0.25 0.18–1.23	bdl	bdl	bdl
Dy	bdl	bdl	5.66 1.09 2.61–7.91	0.42 0.19 <0.1–0.70	bdl	bdl
Ho	bdl	bdl	1.00 0.10 0.75–1.27	bdl	bdl	bdl
Er	bdl	bdl	3.16 0.47 2.2–4.34	bdl	bdl	bdl
Tm	bdl	bdl	0.28 0.09 <0.1–0.49	bdl	bdl	bdl
Yb	bdl	bdl	2.81 1.25 1.19–5.51	bdl	bdl	bdl
Lu	bdl	bdl	0.59 0.16 0.30–1.04	bdl	bdl	bdl

bdl – below detection limit; when the number of points containing a specific element below detection limit amounted to >20% of the total number of points, then only observed concentration ranges are given

trast, the uppermost Triassic and the Lower Jurassic mudstones and claystones of the Polish Basin reveal a negative Eu anomaly varying from 0.48 to 0.70 (mean of 0.64) and 0.53 to 0.68 (mean of 0.63), respectively (Brański and Mikulski, 2016). These low coefficients may suggest the oxidation conditions that prevailed in a shallow sedimentary basin or an influence of different post-depositional processes. However, a lack of detailed mineralogical REE study in many areas makes difficult adequate interpretation of positive or negative Eu anomalies in siliciclastic rock formations (pH/Eh conditions, composition and provenance of REE source material, weathering processes, etc.). The redox Eu signature is also backed up by the mineralogical context of the hosting pyrite mineralization zones. The data indicate that microcrystalline pyrite forms in sediments under euxinic (H_2S abundance and lack of O_2) or intermittent anoxic (lack of H_2S and O_2) conditions, especially in black shale facies enriched in organic matter as a reductant (Schieber, 2001).

Another direct indicator of euxinic-anoxic environments in the Wiśniówka depositional basin is the V/(Ni+V) ratio. Its val-

ues vary mostly from 0.84 to 0.95 occasionally from 0.63 to 0.83 (Migaszewski and Gałuszka, 2019). The former range points to euxinic whereas the latter to anoxic conditions (Hatch and Leventhal, 1992). These short periods of pyrite formation may have reflected the restricted influxes of Fe- and H_2S-rich hydrothermal fluids and the hampered process of bacterial sulfate reduction (BSR) process. Both oxic and dysoxic (low O_2 contents) conditions have not been recorded in clayey-silty facies as opposed to some quartzite beds showing the V/(Ni+V) ratio in the range of 0.08 to 0.51 (Migaszewski and Gałuszka, 2019). This implies that periodical inputs of sandy material, which was supplied by suspension currents from the proximal parts of the shelf into the deeper parts of the Wiśniówka basin, caused variations in the prevailing redox conditions.

Moreover, the lower values of the Eu/Eu$_{NASC}$* coefficient in quartzites/quartzitic sandstones of Wiśniówka Duża (1.04) and Podwiśniówka (1.12) points actually to a lack of Eu anomaly (1.2). This may suggest somewhat oxidizing conditions induced by suspension currents that transported sandy material from proximal parts of the sedimentary basin, which is also evi-

Contents of REEs and major associated elements in selected APS minerals and xenotime of the Wiśniówka area (derived from EMPA)

Element [wt.%]	APS group – WD2 (Fig. 3G)			Xenotime – Pw34 (Fig. 4D)		Xenotime – Pw34 (Fig. 4E)			
	#1	#2	#3	#1	#2	#1	#2	#3	#4
Al	16.36	18.19	16.21	bdl	bdl	bdl	bdl	bdl	bdl
Ba	1.46	4.37	2.18	bdl	bdl	bdl	bdl	bdl	bdl
Ca	1.63	2.22	1.62	bdl	bdl	bdl	0.02	0.07	0.34
Fe	0.51	1.10	1.17	bdl	bdl	bdl	bdl	1.44	bdl
P	11.36	12.61	11.11	14.76	14.69	15.17	15.30	15.32	15.24
S	0.97	0.86	1.52	bdl	bdl	bdl	bdl	bdl	bdl
Sr	4.47	4.14	4.26	bdl	bdl	bdl	bdl	bdl	bdl
Th	bdl	bdl	bdl	0.83	0.47	0.20	0.42	0.48	0.36
U	bdl	bdl	bdl	0.32	0.34	0.22	1.23	0.62	0.35
Y	bdl	bdl	bdl	33.57	33.65	33.23	32.85	32.75	33.66
La	1.89	1.72	1.38	bdl	bdl	bdl	bdl	bdl	bdl
Ce	6.85	5.78	4.71	bdl	bdl	bdl	bdl	bdl	bdl
Pr	bdl	bdl	bdl	bdl	bdl	bdl	bdl	bdl	bdl
Nd	3.10	2.89	2.45	0.26	0.33	0.11	0.37	0.32	0.23
Sm	0.47	0.48	0.41	0.78	0.70	bdl	bdl	bdl	bdl
Eu	bdl	bdl	bdl	0.38	0.40	0.18	bdl	bdl	0.33
Gd	bdl	bdl	bdl	2.69	2.67	2.12	2.24	2.12	2.32
Tb	bdl	bdl	bdl	0.64	0.62	0.61	1.57	1.53	0.63
Dy	bdl	bdl	bdl	5.92	5.74	6.59	5.21	5.19	5.80
Ho	bdl	bdl	bdl	1.13	0.98	1.27	1.06	1.00	1.11
Er	bdl	bdl	bdl	3.04	2.96	3.62	3.53	3.22	3.12
Tm	bdl	bdl	bdl	0.18	0.20	0.31	0.36	0.34	0.25
Yb	bdl	bdl	bdl	1.96	2.03	2.73	3.24	3.22	1.97
Lu	bdl	bdl	bdl	0.54	0.54	0.51	0.53	0.66	0.55
REEs (La-Lu)	12.31	10.87	8.95	17.52	17.17	18.05	18.11	17.60	16.31

bdl – below detection limit (~0.1 wt.%)

denced by the local presence of sandstone balls up to 40 cm in diameter in some quartzite beds (Migaszewski and Gałuszka, 2019). This process may have distorted a distinct Eu anomaly in these detrital rocks. The far lower Eu/Eu_{NASC}^{*} values (range of 0.4 to 0.8; mean of 0.59) have in turn been found in Proterozoic sandstones and quartzites of southeastern India. Hence, the negative Eu anomaly may be indicative of oxidizing conditions in a sedimentary basin (Wani, 2017). This may imply that inputs of detrital material from oxic-dysoxic sandy facies into the deeper euxinic-anoxic muddy facies may have changed the original positive Eu anomaly.

The Ce/Ce_{NASC}^{*} coefficient is too low (1.02 to 1.09) to be recognized as a positive anomaly (1.2) and a proxy for redox conditions due to diverse mixing of hydrothermal vent fluids and seawater during formation of pyrite and REE-rich minerals. The REE geochemical data, but especially strong LREE enrichments in relation to HREE, a positive Eu anomaly associated with weak negative to positive Ce anomalies point to a stronger influence of hydrothermal events (German et al., 1990, 1999; Wang et al., 2012).

MULTIPROXY RECORD FOR HYDROTHERMAL REE-MINERAL PROVENANCE

Another important issue is a source of Al, Ba, Ca, Sr, P, REEs and Y for the formation of REE-rich minerals, especially when considering the REE scarcity (1 to 6.5 mg/kg) in the ocean water (Elderfield and Greaves, 1982). However, the sulfate reduction zone (below the sediment-water interface) may exhibit the 10-to-50 higher levels of REEs (Elderfield and Sholkovitz, 1987). Hydrothermal sediments show in turn higher REE concentrations (in mg/kg levels) than seawater and submarine hydrothermal fluids. Different REE patterns result from competing for the scavenging mechanism in precipitated minerals. The formation of APS and phosphate minerals requires a low pH and high concentrations of dissolved phosphates (Nriagu, 1976; Stoffregen and Alpers, 1987).

There is no indication of magmatic activity within the Wiśniówka siliciclastic depositional basin or the transport of REE-rich minerals (except for scarce monazite inclusions in detrital quartz grains) with suspension current material from the
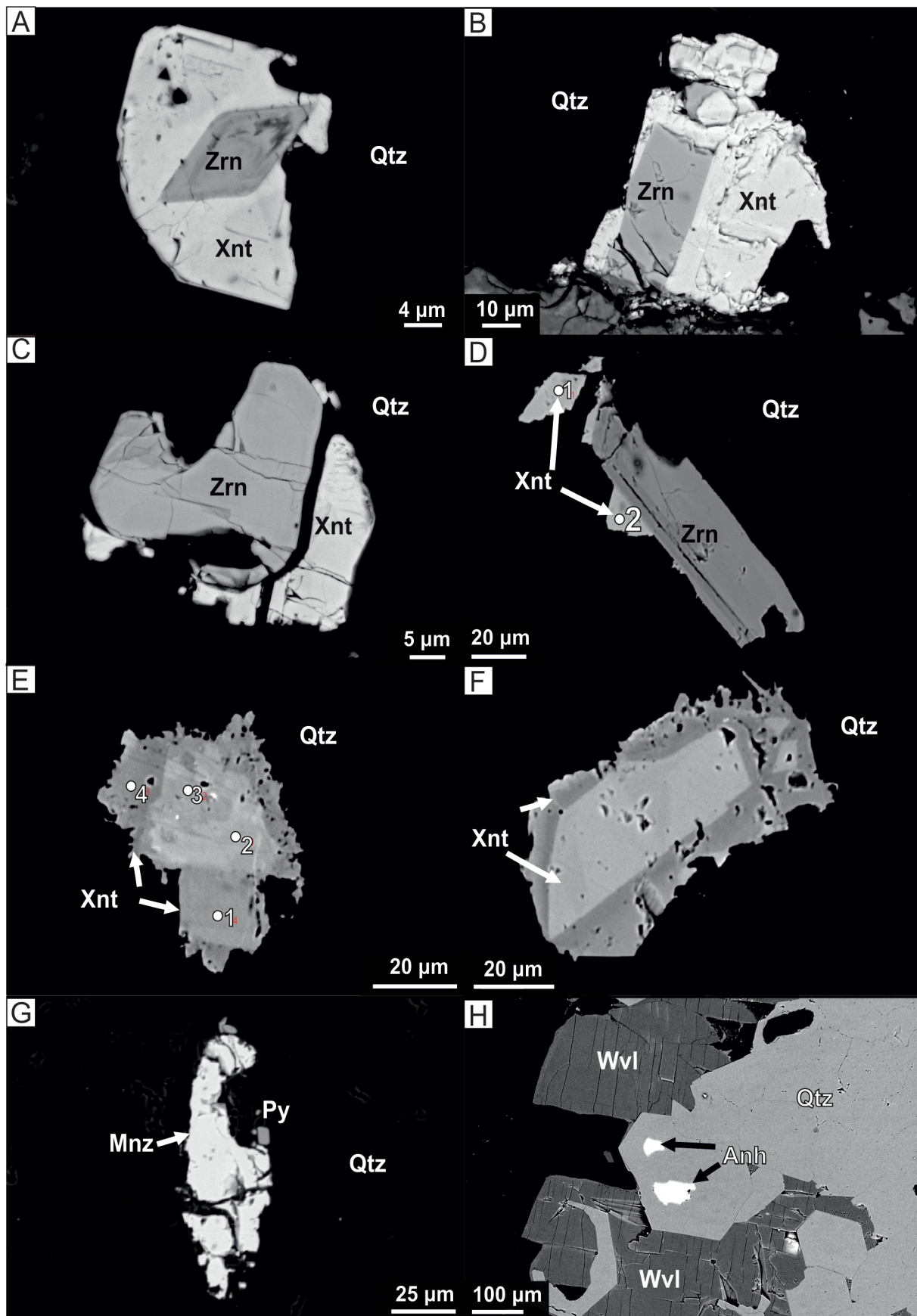
Fig. 4. Back-scattered SEM (A–C) and EMP (D–H) photomicrographs of REE-rich minerals

A, **B**, **C**, **D** – different forms of detrital zircon grains rimmed by HREE-rich xenotime showing zonal and/or patchy microtextures (samples WD2, Pw15, WD2 and Pw34, respectively); **E**, **F** – individual xenotime grains composed of three generations (sample Pw34); **G** – a cracked and etched individual monazite grain with an adjacent pyrite inclusion (sample WD34); **H** – a wavellite assemblage infilling veined quartz microvoids with occasional anhydrite inclusions; explanation as in Figure 3

proximal parts of the shelf. The other processes, e.g., hypogene alterations (including submarine weathering) or supergene processes should not be taken under consideration. Trace amounts of felspar also preclude their degradation as a major source of some elements (Dill, 2001). The other potential source of Al, Ba, Ca, Sr, P, REEs and Y is volcanic ashes that give rise to bentonite/tuffite interbeds in the oldest southern strata of the Podwiśniówka Quarry. However, the pyrite mineralization zones, which occupies the most part of the Wiśniówka geologic profile, practically lacks this volcanoclastic material as indicated by the previous petrographic study (Migaszewski and Gałuszka, 2019).

There is mineralogical evidence suggesting the submarine hot spring origin of REE-bearing minerals. These include common paragenetic assemblages of APS minerals associated with hydrothermal pyrite and nacrite/dickite (Migaszewski and Gałuszka, 2019). The Ariadne's web is Wiśniówka pyrite that shows both extremely high concentrations of As (up to 8.2% based on LA-ICP-MS measurements) and uncommonly negative ^{34}S values (from –41.4 to –19.8‰), fingerprinting sediment-hosted pyrite stratiform deposits (Migaszewski et al., 2008, 2016; Migaszewski and Gałuszka, 2019 and references therein). These highly negative values also suggest that organic matter may have been involved in the formation of pyrite and some REE-rich minerals. The negative ^{34}S (–42.5‰) values of pyrite have also been recorded in fossil hydrothermal chimneys and mounds at Silvermines (Central Ireland; Boyce et al., 1983). The negative stable sulfur signatures are also a proxy for activity of microorganisms preserved in the form of some framboids in the Wiśniówka area (Migaszewski et al., 2018a, b; Migaszewski and Gałuszka, 2019) or microfossils (acritarchs?) infilled with anatase (Migaszewski and Gałuszka, 2023) or goyazite aggregates (Fig. 3E). Hydrothermal origin of pyrite is evidenced not only by an untypical high content of arsenic (uncommon in sedimentary formations), but also by alternating arsenic-rich and arsenic-poor internal microbands in pyrite grains (Kolker and Nordstrom, 2001). This mineralogical and isotopic context also cast light on the origin of REE-bearing minerals. Besides, considerable variations of xenotime overgrowths in size and morphology, and an irregular zonal-patchy microtexture is a characteristic mineralogical signature of hydrothermal activity (Rasmussen, 1996; Kositcin et al., 2003). The same properties are also related to APS minerals that commonly show a zonal-patchy microtexture.

Another hydrothermal proxy for REE-rich minerals is both the predominance of LREEs over HREEs and a positive Eu anomaly that have commonly been found in hydrothermal sea-floor systems, for example in metalliferous sediments and hydrothermal fluids of the Red Sea and the East Pacific Rise (Courtois and Treuil, 1977; Michard et al., 1983; Michard and Albarède, 1986; Douville et al., 1999; German et al., 1990, 1999; Bau and Dulski, 1996; Wang et al., 2012). It is noteworthy that average black and white smoker fluid of the active TAG Mound has shown a strongly positive Eu anomaly and a negligible Ce negative anomaly with LREE enrichments as opposed to ambient sea water that has exhibited a weak negative Eu anomaly and a distinctly negative Ce anomaly with HREE enrichments (Mills and Elderfield, 1995). Because Wiśniówka siliciclastic rocks are not metamorphic in origin (except for some negligible parts of white quartzites which are devoid of REEs), the REE patterns reflect the REE composition of fluids. The occurrence of different REE-minerals and resultant diverse contents of REEs and Y between individual beds also suggest variable geochemistry and periodical influxes of hydrothermal fluids discharged into the seafloor sediment and the water column. The geochemical fluid diversity is evidenced by enrichments of goyazite and gorceixite (vs. xenotime and monazite) in Cl and F. This may indicate that aqueous complexes of these two elements have played a significant role in transporting REEs and crystallization of APS minerals (Williams-Jones and Artas, 2014).

It is hard to establish the sequence of mineral crystallization in the Wiśniówka siliciclastic series due to multiphase formation of pyrite, APS and phosphate minerals, and nacrite/dickite, not to mention TiO_2 polymorphs (rutile, anatase, brookite). Pyrite and nacrite/dickite aggregations and veinlets seem to have crystallized prior to REE-bearing assemblages although locally a reverse sequence is observed. This means that it is reasonable to assume that all these minerals, which occur in the pyrite mineralization zones, may be recognized as nearly coeval. However, REE-depleted variscite and wavellite, co-occurring with quartz veinlets, may have followed the crystallization of APS minerals.

CONCLUSIONS

The Wiśniówka Upper Cambrian Formation takes up a unique position among siliciclastic formations of Poland due to the presence of arsenical pyrite and REE mineralization, which is unusual in hard rock mining worldwide. This and the previous geochemical, mineralogical and petrographic studies combined with stable sulfur isotope measurements have indicated hydrothermal provenance of pyrite, nacrite/dickite and associated REE-rich minerals (Migaszewski and Gałuszka, 2010, 2019). The hot spring fluids discharged Al, Ba, Ca, Sr, P, REEs and Y into the sediment and the seawater column during the Late Cambrian, overprinting the other possible minor sources of these elements. An observed decrease in contents of arsenical pyrite and REE-rich minerals (especially APS minerals) along with the diminishing V/(Ni+V) ratio in the Wiśniówka Duża lithofacies point to vanishing Fe-As-REE mineralization and a gradual shift from euxinic/anoxic toward dysoxic/oxic conditions.

This investigation has documented a broad range of REE-bearing minerals showing different microtextural and geochemical characteristics. There is a lesson that can be drawn from this REE mineralization study. This implies that the use of a variety of analytical techniques combined with field observations enable pinpointing a true source of REEs. This approach has allowed us to determine a hydrothermal origin of REE-rich minerals that are closely related to the pyrite mineralization zones and exclude a major contribution of other potential terrigenous or volcanogenic sources as well as resultant remobilization of REEs from detrital ingredients, organically-coated clay minerals or volcanic ashes. The practical aspect of this study, however, is the potential of the Upper Cambrian Wiśniówka massif for a search of REE mineralization of economic value.

REFERENCES

Acar, A., Sarý, A., Sonel, N., Aliyev, S., 2007. Source rock characterization and depositional environment of the late Cretaceous Haymana formation in the salt lake basin of Turkey. Energy Sources, Part A, **29**: 277–291; https://doi.org/10.1080/009083190965758

Atlas of Eh-pH diagrams: Intercomparison of thermodynamic databases, 2005. National Institute of Advanced Industrial Science and Technology. Research Center for Deep Geological Environments. Naoto TAKENO.

Bau, M., Dulski, P., 1996. Distribution of yttrium and rare-earth elements in the Penge and Kuruman Iron-Formations, Transvaal Supergroup, South Africa. Precambrian Research, **79**: 37–55; https://doi.org/10.1016/0301-9268(95)00087-9

Bełka, Z., Ahrendt, H., Franke, W., Buła, Z., Jachowicz, M., Wemmer, K., 1997. Accretion of pre-Variscan terranes in the Trans-European Suture Zone: evidence from K/Ar ages of detrital muscovites. Terra Nova, **970**: 21–23.

Boyce, A.J., Coleman, M.L., Russel, M.J., 1983. Formation of fossil hydrothermal chimneys and mounds from Silvermines, Ireland. Nature, **306**: 545–550; https://doi.org/10.1038/306545a0

Brański, P., Mikulski, S.Z., 2016. Rare earth elements distribution in fine-grained deposits from the uppermost Triassic and Lower Jurassic of the Polish Basin: provenance and weathering in the source area. Geological Quarterly, **60** (2): 441–450; https://doi.org/10.7306/gq.1288

Brookins, D.G., 1989. Aqueous geochemistry of rare earth elements. Review in Mineralogy, **8**: 201–225; https://doi.org/10.1515/9781501509032-011

Chakhmouradian, A.R., Wall, F., 2012. Rare earth elements: Minerals, mines, magnets (and more). Elements, **8**: 333–340; https://doi.org/10.2113/gselements.8.5.333

Courtois, C., Treuil, M., 1977. Distribution des terres rares et de quelques éléments en trace dans les sédiments récents des fosses de la Mer Rouge. Chemical Geology, **20**: 57–72; https://doi.org/10.1016/0009-2541(77)90035-3

Dia, A., Gruau, G., Olivie-Lauquet, G., Riou, C., Molenat, J., Curmi, P., 2000. The distribution of rare earth elements in groundwaters; assessing the role of source–rock composition, redox changes and colloidal particles. Geochimica et Cosmochimica Acta, **64**: 4131–4151; https://doi.org/10.1016/S0016-7037(00)00494-4

Dill, H.G., 2001. The geology of aluminium phosphates and sulphates of the alunite group minerals: a review. Earth-Science Reviews, **53**: 35–93; https://doi.org/10.1016/S0012-8252(00)00035-0

Douville, E., Bienvenu, P., Charlou, J. L., Donval, J. P., Fouquet, Y., Appriou, P., Gamo, T., 1999. Yttrium and rare earth elements in fluids from various dep-sea hydrothermal systems. Geochimica et Cosmochimica Acta, **55**: 3553–3558; https://doi.org/10.1016/S0016-7037(99)00024-1

Elderfield, H., Greaves, M.J., 1982. The rare earth elements in sea water. Nature **296**: 214–219; https://doi.org/10.1038/296214a0

Elderfield, H., Sholkovitz, E.R., 1987. Rare earth elements in the pore waters of reducing nearshore sediments. Earth and Planetary Science Letters, **82**: 280–288; https://doi.org/10.1016/0012-821X(87)90202-0

Emsbo, P., McLaughlin, P.I., Breit, G.N., du Bray, E.A., Koenig, A.E., 2015. Rare earth elements in sedimentary phosphate deposits: Solution to the global REE crisis? Gondwana Research, **27**: 776–785; https://doi.org/10.1016/j.gr.2014.10.008

Gałuszka, A., Migaszewski, Z.M., Pelc, A., Trembaczowski, A., Dołęgowska, S., Michalik, A., 2020. Trace elements and stable sulfur isotopes in plants of acid mine drainage area: Implications for revegetation of degraded land. Journal of Environmental Sciences, **94**: 128–136; https://doi.org/10.1016/j.jes.2020.03.041

German, C.R., Klinkhammer, G.P., Edmond, J.M., Mitra, A., Elderfield, H., 1990. Hydrothermal scavenging of rare earth elements in the ocean. Nature, **345**: 516–518; https://doi.org/10.1038/345516a0

German, C.R., Hollday, B.P., Elderfield, H., 1991. Redox cycling of rare earth elements in the suboxic zone of the Black Sea. Geochimica et Cosmochimica Acta, **55**: 3553–3558; https://doi.org/10.1016/0016-7037(91)90055-A

German, C.R., Hergt, J., Palmer, M.R., Edmond, J.M., 1999. Geochemistry of hydrothermal sediment core from the OBS vent field, 21°N East Pacific Rise. Chemical Geology, **155**: 65–75; https://doi.org/10.1016/S0009-2541(98)00141-7

Grawunder, A., Merten, D., Büchel, G., 2014. Origin of middle rare earth element enrichment in acid mine drainage-impacted areas. Environmental Science and Pollution Research, **21**: 6812–6823; https://doi.org/10.1007/s11356-013-2107-x

Gromet, L.P., Dymek, R.F., Haskin, L.A., Korotev, R.L., 1984. The "North American shale composite"; its compilation, major and trace element characteristics. Geochimica et Cosmochimica Acta, **48**: 2469–2482; https://doi.org/10.1016/0016-7037(84)90298-9

Harlov, D.E., Procházka, V., Förster, H.-J., Matějka, D., 2008. Origin of monazite–xenotime–zircon–fluorapatite assemblages in the peraluminous Melechov granite massif, Czech Republic. Mineralogy and Petrology, **94**: 9–26; https://doi.org/10.1007/s00710-008-0003-8

Haskin, L.A., Wildeman, T.R., Haskin, M.A., 1968. An accurate procedure for the determination of the rare earths by neutron activation. Journal of Radioanalytical and Nuclear Chemistry, **1**: 337–348; https://doi.org/10.1007/bf02513689

Hatch, J.R., Leventhal, J.S., 1992. Relationship between inferred redox potential of the depositional environment and geochemistry of the Upper Pennsylvanian (Missourian) Stark Shale member of the Dennis Limestone, Wabaunsee County, Kansas, USA. Chemical Geology, **99**: 65–82; https://doi.org/10.1016/0009-2541(92)90031-Y

Hetherington, C.J., Jercinovic, M.J., Williams, M.L., Mahan, K., 2008. Understanding geologic processes with xenotime: Composition, chronology, and a protocol for electron probe microanalysis. Chemical Geology, **254**: 133–147; https://doi.org/10.1016/j.chemgeo.2008.05.020

Jaworowski, K., Sikorska, M., 2006. Łysogóry Unit (Central Poland) versus East European Craton – application of sedimentological data from Cambrian siliciclastic association. Geological Quarterly, **50** (1): 77–88.

Koç, S., Sarý, A., Çimen, O., 2016. Major and rare earth element contents in sedimentary rocks of Haymana formation, Ankara, Turkey. Energy Sources, part A: Recovery, Utilization, and Environmental Effects, **38**: 1918–1928; https://doi.org/10.1080/15567036.2014.967418

Kolker, A., Nordstrom, D.K., 2001. Occurrence and micro-distribution of arsenic in pyrite. USGS Workshop on Arsenic in the Environment, Feb. 21–22, 2001, Denver, CO. Extended abstracts: 1–3; http://wwwbrr.cr.usgs.gov/Arsenic/

Konon, A., 2008. Tectonic subdivision of Poland: Holy Cross Mountains and adjacent areas (in Polish). Przegląd Geologiczny, **56**: 921–926.

Kositcin, N., McNaughton, N.J., Griffin, B.J., Fletcher, I.R., Groves, D.I., Rasmussen, B., 2003. Textural and geochemical discrimination between xenotime of different origin in the Archaean Witwatersrand Basin, South Africa. Geochimica et Cosmochimica Acta, **67**: 709–731; https://doi.org/10.1016/S0016-7037(02)01169-9

Leybourne, M.I., Goodfellow, W.D., Boyle, D.R., Hall, G.M., 2000. Rapid development of negative Ce anomalies in surface waters and contrasting REE patterns in groundwaters associated with Zn-Pb massive sulphide deposits. Applied Geochemistry, **15**: 695–723; https://doi.org/10.1016/S0883-2927(99)00096-7

Mazur, S., Mikołajczak, M., Krzywiec, P., Malinowski, M., Buffenmyer, V., Lewandowski, M., 2015. Is the Teysseyre-Tornquist Zone an ancient plate boundary of Baltica? Tectonics, **34**: 2465–2477; https://doi.org/10.1002/2015TC003934

Michard, A., Albarède, F., 1986. The REE content of some hydrothermal fluids. Chemical Geology, **55**: 51–60; https://doi.org/10.1016/0009-2541(86)90127-0

Michard, A., Albarède, F., Michard, G., Minster, J.F., Charlou, J.L., 1983. Rare-earth elements and uranium in high-temperature solutions from East Pacific Rise hydrothermal vent field (13°N). Nature, **303**: 795–797; https://doi.org/10.1038/303795a0

Miekeley, N., Couthino de Jesus, H., Porto da Silveira, C.L., 1992. Rare earth elements in groundwater from the Osamu Utsumi mine and Morro do Ferro analogue study sites, Plcos de Caldas, Brazil. Journal of Geochemical Exploration, 45: 365–387; https://doi.org/10.1016/0375-6742(92)90131-Q

Migaszewski, Z.M., Gałuszka, A., 2010. Xenotime from the Podwiśniówka mine pit, Holy Cross Mountains (South-Central Poland). Mineralogia, 41 (1–2): 1–7; https://doi.org/10.2478/v10002-010-0007-y

Migaszewski, Z.M., Gałuszka, A., 2015. The characteristics, occurrence and geochemical behavior of rare earth elements in the environment: a review. Critical Reviews in Environmental Science and Technology, 45: 429–471; https://doi.org/10.1080/10643389.2013.866622

Migaszewski, Z.M., Gałuszka, A., 2019. The origin of pyrite mineralization: Implications for Late Cambrian geology of the Holy Cross Mountains (south-central Poland). Sedimentary Geology, 390: 45–61; https://doi.org/10.1016/j.sedgeo.2019.07.004

Migaszewski, Z.M., Gałuszka, A., 2023. Hydrothermal TiO_2 polymorphs in a pyrite stratiform deposit: lessons from a mineralogical and geochemical multiproxy record. Chemical Geology, 632: 121551; https://doi.org/10.1016/j.chemgeo.2023.121551

Migaszewski, Z.M., Starnawska, E., Gałuszka, A., 2007. Gorceixite from the Upper Cambrian rocks of the Podwiśniówka mine pit, Holy Cross Mountains (south-central Poland). Mineralogia Polonica, 38: 171–184; https://doi.org/10.2478/v10002-007-0025-6

Migaszewski, Z.M., Gałuszka, A., Hałas, S., Dołęgowska, S., Dąbek, J., Starnawska, E., 2008. Geochemistry and stable sulfur and oxygen isotope ratios of the Podwiśniówka pit pond water generated by acid mine drainage (Holy Cross Mountains, south-central Poland). Applied Geochemistry, 23: 3620–3634; https://doi.org/10.1016/j.apgeochem.2008.09.001

Migaszewski, Z.M., Gałuszka, A., Michalik, A., Dołęgowska, S., Migaszewski, A., Hałas, S., Trembaczowski, A., 2013. The use of stable sulfur, oxygen and hydrogen isotope ratios as geochemical tracers of sulfates in the Podwiśniówka acid drainage area (South-Central Poland). Aquatic Geochemistry, 19: 261–280; https://doi.org/10.1007/s10498-013-9194-7

Migaszewski, Z.M., Gałuszka, A., Dołęgowska, S., 2016. Rare earth and trace element signatures for assessing an impact of rock mining and processing on the environment: Wiśniówka case study, south-central Poland. Environmental Science and Pollution Research, 23: 24943–24959; https://doi.org/10.1007/s11356-016-7713-y

Migaszewski, Z.M., Gałuszka, A., Dołęgowska, S., 2018a. Stable isotope geochemistry of acid mine drainage from the Wiśniówka area (south-central Poland). Applied Geochemistry, 95: 45–56; https://doi.org/10.1016/j.apgeochem.2018.05.015

Migaszewski, Z.M., Gałuszka, A., Dołęgowska, S., 2018b. Arsenic in the Wiśniówka acid mine drainage area (south-central Poland) – mineralogy, hydrogeochemistry, remediation. Chemical Geology, 493: 491–503; https://doi.org/10.1016/j.chemgeo.2018.06.027

Migaszewski, Z.M., Gałuszka, A., Dołęgowska, S., 2019. Extreme enrichment of arsenic and rare earth elements in acid mine drainage: Case study of Wiśniówka mining area (south-central Poland). Environmental Pollution, 244: 898–906; https://doi.org/10.1016/j.envpol.2018.10.106

Mikulski, S.Z., Brański, P., Pieńkowski, G., Małek, R., Zglinicki, K., Chmielewski, A., 2021. REE enrichment of sedimentary formations in selected regions of the Mesozoic margin of the Holy Cross Mountains – promising preliminary data and more research needed (in Polish with English summary). Przegląd Geologiczny, 69: 379–385; http://dx.doi.org/10.7306/2021.21

Mills, R.A., Elderfield, H., 1995. Rare earth element geochemistry of hydrothermal deposits from the active TAG mound, 26°N Mid-Atlantic Ridge. Geochimica et Cosmochimica Acta, 59: 3511–3524; https://doi.org/10.1016/0016-7037(95)00224-N

Moreno-González, R., Cánovas, C.R., Olías, M., Macías, F., 2020. Seasonal variability of extremely metal rich acid mine drainages from the Tharsis mines (SW Spain). Environmental Pollution, 259, 113829; https://doi.org/10.1016/j.envpol.2019.113829

Nriagu, J.O., 1976. Phosphate – clay mineral relations in soils and sediments. Canadian Journal of Earth Science, 13: 717–736; https://doi.org/10.1139/e76-077

Orłowski, S., 1975. Cambrian and Upper Precambrian lithostratigraphic units in the Holy Cross Mts. (in Polish) Acta Geologica Polonica, 25: 431–448.

Rasmussen, B., 1996. Early-diagenetic REE-phosphate minerals (florencite, crandallite, gorceixite and xenotime) in marine sandstones: A major sink for oceanic phosphorus. American Journal of Science, 296: 601–632; https://doi.org/10.2475/ajs.296.6.601

Rasmussen, B., 2005. Radiometric dating of sedimentary rocks: the application of diagenetic xenotime geochronology. Earth-Science Reviews, 68: 197–243; https://doi.org/10.1016/j.earscirev.2004.05.004

Rasmussen, B., Buick, R., Taylor, W.R., 1998. Removal of oceanic REE by authigenic precipitation of phosphatic minerals. Earth and Planetary Science Letters, 164: 135–149; https://doi.org/10.1016/S0012-821X(98)00199-X

Rasmussen, B., Fletcher, I.R., Muhling, J.R., Thorne, W.S., Broadbent, G.C., 2007. Prolonged history of episodic fluid flow in giant hematite ore bodies: Evidence from in situ U–Pb geochronology of hydrothermal xenotime. Earth and Planetary Science Letters, 258: 249–259; https://doi.org/10.1016/j.epsl.2007.03.033

Richter, D.K., Krampitz, H., Görgen, P., Götte, T., Neuser, R.D., 2006. Xenotime in the Lower Buntsandstein of Central Europe: Evidence from cathodoluminescence investigation. Sedimentary Geology, 183: 261–268; https://doi.org/10.1016/j.sedgeo.2005.09.017

Sawłowicz, Z., 2013. REE and their relevance to the development of the Kupferschiefer copper deposits in Poland. Ore Geology Reviews, 55: 176–186; https://doi.org/10.1016/j.oregeorev.2013.06.006

Schieber, J., 2001. A role for organic petrology in integrated studies of mudrocks: examples from Devonian black shales of the eastern US. International Journal of Coal Geology, 47: 171–187; https://doi.org/10.1016/S0166-5162(01)00041-6

Stanisławska, M., Michalik, M., 2008. Xenotime-(Y) veins in a Neoproterozoic metamudstone (Małopolska Block, S. Poland). Mineralogia, 39: 105–113; https://doi.org/10.2478/v10002-008-0008-2

Stoffregen, R.F., Alpers, C.N., 1987. Woodhouseite and svanbergite in hydrothermal ore deposits: product of apatite destruction during advanced argillic alteration. Canadian Mineralogist, 2: 201–211.

Taylor, S.R., McLennan, S.M., 1985. The Continental Crust: Its Composition and Evolution. Blackwell Scientific, Oxford, Melbourne.

Vallini, D.A., Rasmussen, B., Krapez, B., Fletcher, I.R., McNaughton, N.J., 2005. Microtextures, geochemistry and geochronology of authigenic xenotime: constraining the cementation history of a Palaeoproterozoic metasedimentary sequence. Sedimentology, 52: 101–122; https://doi.org/10.1111/j.1365-3091.2004.00688.x

Wang, J., Chen, D., Wang, D., Yan, D., Zhou, X., Wang, Q., 2012. Petrology and geochemistry of chert on the marginal zone of Yangtze Platform, western Hunan, South China, during the Ediacaran–Cambrian Transition. Sedimentology, 59: 809–829; https://doi.org/10.1111/j.1365-3091.2011.01280.x

Wani, H., 2017. REE Characteristics and REE mixing modeling of the Proterozoic quartzites and sandstones. International Journal of Geosciences, 8: 16–29; http://dx.doi.org/10.4236/ijg.2017.81002

Wedepohl, K.H., 1995. The composition of the continental crust. Geochimica et Cosmochimica Acta 59: 1217–1232; https://doi.org/10.1016/0016-7037(95)00038-2

William-Jones, E.A., Artas, M.A., 2014. Rare earth element transport and deposition by hydrothermal fluids. Acta Geologica Sinica, 88: 472–474; https://doi.org/10.1111/1755-6724.12373_28

Żylińska, A., Szczepanik, Z., Salwa, S., 2006. Cambrian of the Holy Cross Mountains, Poland: biostratigraphy of the Wiśniówka Hill succession. Acta Geologica Polonica, 56: 443–461.